An Assessment of RASSCF and TDDFT Energies and Gradients on an Organic Donor−Acceptor Dye Assisted by Resonance Raman Spectroscopy

Stephan Kupfer,[†] Julien Guthmuller,[‡] and Leticia González*,[§]

[†]Institute for Physical Chemistry, Friedrich-Schiller University Jena, Helmholtzweg 4, 07743 Jena, Germany
[‡]Faculty of Applied Physics and Mathematics, Gdansk University of Technology, Narutowicza 11/12, 80233 Gdansk, Poland
[§]Institute of Theoretical Chemistry, University of Vienna, Währinger Str. 17, 1090 Vienna, Austria

S Supporting Information

ABSTRACT: The excitation energies and gradients in the ground and the first excited state of a novel donor−(π-bridge)−acceptor 4-methoxy-1,3-thiazole-based chromophore were investigated by means of MS-RASPT2/RASSCF and TDDFT in solution. Within both methods, the excitation energies strongly depend on the employed equilibrium structures, whose differences can be rationalized in terms of bond length alternation indexes. It is shown that functionals with an increased amount of exact exchange provide the best estimation of the ground and excited state properties. While B3LYP fails to predict the excitation energies due to its intrinsic problems in describing charge transfer (CT) states, the long-range corrected CAM-B3LYP and M06-2X functionals deliver good agreement with the experimental UV/vis absorption spectrum. The calculation of resonance Raman intensity patterns is used to discern which ground and excited state gradients are best. The results clearly evidence that both CAM-B3LYP and RASSCF excited state gradients and energies in combination with CAM-B3LYP ground state gradients are appropriate to describe the CT state of this push−pull chromophore.
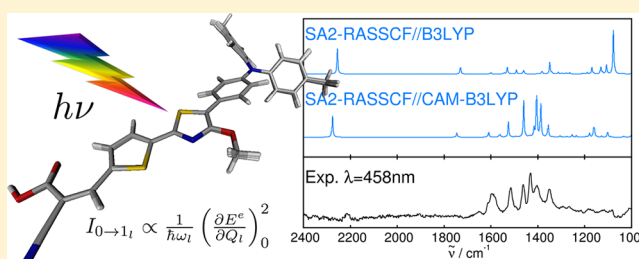
1. INTRODUCTION

The evaluation of molecular properties in the electronic ground state, e.g. energies, equilibrium structures and dipole moments, can be considered nowadays almost routine, at least in the case of small and medium sized organic systems. In these situations, the electronic ground state is often described by density functional theory (DFT) methods. In particular, hybrid functionals have proven very useful as they can give an accurate description of equilibrium geometries, potential energy surfaces, and dipole moments in various chemical situations, see e.g., refs 1−4.

More challenging however is the simulation of electronic excited states properties, such as excitation energies and transition dipole moments.[5−7] In particular, the investigation of excited states involving charge transfer (CT) character is a difficult task.[7−10] Multiconfigurational methods, such as the recently developed RASPT2[11,12]/RASSCF[13,14] (Restricted Active Space Perturbation Theory of second order/Restricted Active Space Self-Consistent Field) or the well-established CASPT2[15]/CASSCF[16] (Complete Active Space Perturbation Theory of second order/Complete Active Space SCF) approaches are able to deliver a reliable description of excited states, irrespective of the character of the wave functions. While in the CASSCF method the orbitals are classified into inactive, active, and secondary orbitals, in the RASSCF the active orbitals are further divided into three subspaces, RAS1, RAS2,

and RAS3, bringing additional flexibility to the wave function. The orbitals in the RAS2 subspace keep the same meaning as in the active space of CASSCF (i.e., a full configuration interaction (CI) calculation is performed), and the RAS CI is built by restricting the number of holes in RAS1 and particles in RAS3, typically by two or three. In this way, a wise choice of the RAS subspaces can drastically reduce the number of configuration state functions (CSFs) and therefore the computational demand, in comparison to CASSCF. Alternatively, for the same computational effort as in a CASSCF calculation, RASSCF allows for extending the number of active orbitals by restricting the excitation level and therefore can be used in larger systems or those demanding larger active spaces. Recently, the performance of RASPT2/RASSCF has been benchmarked in a number of organic molecules[11,17,18] and was shown to provide accurate results.

Despite the promising advantages of multiconfigurational procedures, the gold standard to calculate excited states of medium or large molecular systems is by far the more economical time-dependent DFT (TDDFT)[19] method. An acute problem of TDDFT is that in the case of CT states it gives poor predictions of excitation energies.[20] To palliate this deficiency, range-separated functionals, such as CAM-B3LYP,[21]

and global hybrid functionals[22] with an enhanced ratio of exact-exchange, such as M06-2X,[23] have been recently developed. A good number of papers can be found in the literature devoted to investigating the performance of different functionals in such complicated cases.[7,8,24−28]

While a lot of studies deal with excited state energies, much less is known of the performance of quantum chemical methods concerning excited state gradients[29] and excited state equilibrium geometries.[30−33] Excited state gradients are fundamental to exploring potential energy surfaces, e.g., in light-induced processes, but also are the main ingredients for optical quantity in emission and resonance Raman (RR) spectroscopy, which is extremely useful in providing relationships between the geometrical structures and the electronic character of the states.[18,29,34] In particular, the RR intensities of the vibrational modes are directly correlated to the excited state gradients in the Franck−Condon (FC) region. Thus, the comparison of simulated and experimental RR spectra provides a unique scenario to evaluate the accuracy of calculated excited state gradients. Several studies have reported calculations of RR spectra for organic compounds (see e.g. refs 29, 35−40) or for transition metal complexes (see e.g. refs 18, 34, 41−43 and references herein). These studies mostly made use of TDDFT but very rarely made use of wave function based methods.

In the present study, the 2-cyano-3-(5-(5-(4-(dip-tolylamino)phenyl)-4-methoxythiazol-2-yl)thiophen-2-yl)-acrylic acid[32] dye (see **1** in Figure 1) is chosen as a large organic
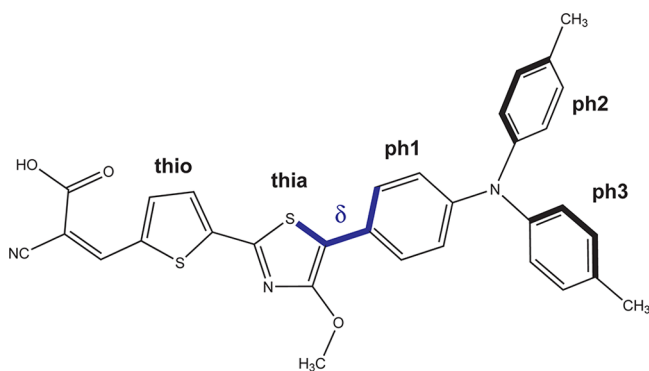

Figure 1. Structure of **1** comprising the labels of the thiophene (thio), thiazole (thia), and the phenyl moieties (ph1, ph2, and ph3) of the donor group. The dihedral angle δ describes the torsion between the bridge and the donor subunits.

chromophore to benchmark excited state gradients in the context of RR spectroscopy. The donor−(π-conjugated bridge)−acceptor 4-methoxy-1,3-thiazole chromophore is based on the naturally occurring luciferin and has found multiple applications as a light-harvesting ligand in ruthenium-(II) polypyridyl complexes,[33,44] as emissive materials in molecular electronics,[45,46] as fluorescent probes in biochemical applications,[47] in organic light-emitting diodes,[48] as blue-emitters in polymer backbones,[49] as nonlinear optical materials,[50,51] as dyes for Förster resonance energy transfer,[52] and as chromophores in dye-sensitized solar cells.[32] Because the thiazole dye **1** shows an intense absorption band in the visible region resulting from a CT excitation,[32] it constitutes an excellent reference compound to challenge multiconfigurational and TDDFT methods. In the present work, the first application of the multiconfigurational RASSCF method to the calculation of RR intensities is reported. The RR spectrum of compound **1**

in resonance with the first absorption band is calculated with both RASSCF and TDDFT methods. The results are compared to experimental data, allowing the identification of the functional which is best suited to describe the ground state properties of dye **1**, as well as whether RASSCF alone is suitable to calculate RR intensities.

2. COMPUTATIONAL DETAILS

2.1. Quantum Chemistry. In order to simulate optical properties, an adequate molecular structure is essential since small changes in the ground state geometry can lead to significant differences in the optical properties. This is especially true in the case of conjugated push−pull chromophores like **1**. The ground state equilibrium geometry was optimized by means of DFT using three different functionals with a different amount of exact exchange: the global hybrid functionals B3LYP[53,54] and M06-2X[23] and the long-range corrected CAM-B3LYP[21] functional. The 6-31G-(d,p)[55] double-ζ basis set was employed in combination with all of the functionals. A harmonic vibrational analysis was carried out at the same level of theory to confirm that the obtained structures are minima of the potential energy surface. Because experimental data to sustain the calculated RR spectra are available in solution (chloroform, ε = 4.711, n = 1.445), both the geometries and the vibrational frequencies are calculated using the equilibrium procedure of the integral equation formalism of the polarizable continuum model (IEFPCM).[6]

Vertical excitation energies and oscillator strengths were calculated using TDDFT as well as the multistate (MS) version of RASPT2/RASSCF. The TDDFT calculations are performed over the lowest 10 singlet excited states using the three functionals B3LYP, M06-2X, and CAM-B3LYP with the same basis set as for the ground state properties and are carried out on their respective ground state geometries. These calculations are referred to as TD-B3LYP//B3LYP, TD-M06-2X//M06-2X, and TD-CAM-B3LYP//CAM-B3LYP. Additionally, a TDDFT calculation employing CAM-B3LYP was performed on the B3LYP equilibrium geometry—this is denoted as TD-CAM-B3LYP//B3LYP. Gaseous as well as solvated (chloroform with IEFPCM) excited state properties have been considered to assess the influence of the solvent. In the case of the solvated compound, the excitation energies and excited state gradients have been calculated with the nonequilibrium procedure of IEFPCM. This treatment is well adapted for the processes of absorption and RR, for which only the fast reorganization of the electronic distribution of the solvent is important.

The MS-RASPT2/RASSCF calculations employed the atomic natural orbitals small basis set (ANO-S)[56] with the contractions S[7s7p4d]/C,N,O[3s2p1d]/H[2s1p]. The Cholesky decomposition[57] was applied to generate the two-electron integrals. The calculations were performed on two solvated DFT equilibrium geometries (B3LYP and CAM-B3LYP) since, as it will be shown, the results show a pronounced dependency of the excitation energy on the geometry (about 0.2 eV). Four different partitions were considered within the RASSCF calculations using different sizes and excitation levels, comprising up to 700.000 CSFs.

In order to label the RAS calculations, the notation RAS($n,l,m;i,j,k$) of Gagliardi and co-workers[17] is used. The index n labels the number of active electrons, l is the maximum number of holes in the RAS1, and m is the maximum number of electrons in the RAS3. The labels i, j, and k refer to the number of active orbitals in the RAS1, RAS2, and RAS3,
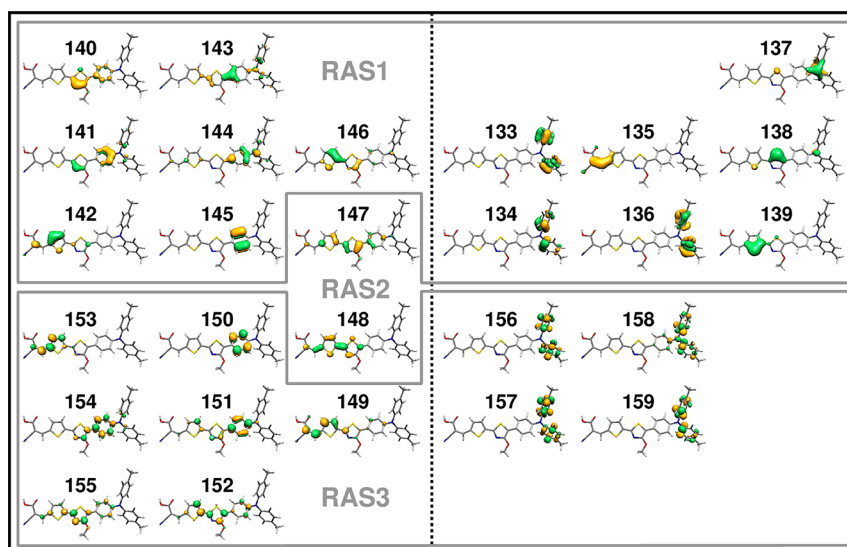
Figure 2. Molecular orbitals for RASSCF(30,2,2;14,2,11) (solid gray), RASSCF(16,2,2;7,2,7), RASSCF(16,3,3;7,2,7), and RASSCF(16,4,4;7,2,7) (left-hand side) calculations.

respectively. The RAS1 includes typically orbitals with large occupation numbers, where only a maximal number of electron holes is allowed. Accordingly, the RAS3 subspace comprises virtual orbitals with small occupation numbers, where only a maximal number of electrons is allowed. In the RAS2 subspace, all possible configurations are taken into account.

In order to describe the UV/vis absorption spectrum of **1** the orbitals of the π systems of the donor group (triphenylamine), the bridge (thiazole and thiophene), and the acceptor (ethylene, 2-cyanoacrylic acid) need to be considered. Furthermore, contributions of the two nitrogen lone pairs (triphenylamine and thiazole) and of the p orbitals in the molecular plane of the two sulfur atoms (thiazole and thiophene) should also be taken into account (cf. Figure 1). This makes a total amount of 42 electrons in 38 orbitals, which even for RASSCF would be a formidable task. Therefore, several restrictions were made in designing the active space: (i) The contributions of the donor group were estimated only by the three pairs of π_{ph1} orbitals, two pairs of π_{ph2} and π_{ph3} orbitals, and the nitrogen lone pair. (ii) In the case of ph2 and ph3 moieties, the lowest occupied π_{ph2}/π_{ph3} and highest unoccupied π_{ph2}^*/π_{ph3}^* molecular orbitals (MO) were excluded because these molecular groups contribute only marginally to the S_1 state. (iii) In the π-conjugated bridge, the entire π/π^* systems of the thiazole and thiophene were included (two pairs of π/π^* orbitals, respectively); in addition, the lone pairs of the nitrogen and the two sulfur atoms were considered. (iv) The contribution of the 2-cyanoacrylic acid-acceptor group was reduced to the π/π^* orbitals of the ethylene.

Under these constraints, the active space is reduced to 27 orbitals with 30 electrons that can be redistributed to the three subspaces as follows: The HOMO and LUMO (within the canonical formulation of SCF or DFT calculations) are assigned to the RAS2 and the remaining occupied and unoccupied orbitals were distributed in the RAS1 and RAS3, respectively. We note that the approach of considering only HOMO and LUMO in the RAS2, while distributing the rest of orbitals within RAS1 and RAS3 has been shown to be successful by Gagliardi and co-workers in the case of organic molecules.[17] The orbitals of the resulting RASSCF-(30,2,2;14,2,11) calculation are depicted in Figure 2.

An additional RASSCF partition was considered taking the entire π/π^* systems of the bridge and the ph1-moiety. Due to the orbital mixing with one π orbital of ph2/ph3 and the π^* of the ethylene, an active space collecting 16 electrons in 16 orbitals was created. Those orbitals were distributed over the three RAS subspaces applying different excitation levels (see Figure 2): In the RAS(16,2,2;7,2,7), the HOMO and the LUMO were assigned to the RAS2. The remaining orbitals were assigned to the RAS1 and RAS3, and only single and double excitations are considered. The RAS(16,3,3;7,2,7) and RAS(16,4,4;7,2,7) prescriptions share the same orbital partition but allow up to triple and quadruple excitations, respectively. All RASSCF wave functions are obtained through state-average (SA) calculations over two roots with equal weight. Dynamical correlation was included by performing MS-RASPT2 to improve the energies. In all the MS-RASPT2 calculations, the core electrons were kept frozen. The oscillator strengths have been obtained at the RASSCF and MS-RASPT2 levels of theory with the CAS State Interaction method.[58]

The excited state gradients required to calculate RR intensities are calculated at both the TDDFT and RASSCF levels of theory with the same specifications as the excitation energies. The structural and TDDFT electronic data were obtained using the Gaussian 09 program.[59] The MS-RASPT2/RASSCF calculations were performed with the Molcas 7.8[60−62] software.

2.2. Resonance Raman. The relative RR intensities for an excitation in resonance with the first absorption band were obtained within the short-time approximation (STA).[63] In particular, this approach was recently applied to the molecule of o-nitrophenol[29] to assess the accuracy of calculated excited state gradients. In the STA, the RR intensity for a fundamental transition $0 \rightarrow 1_l$ is calculated from the partial derivative of the excited state electronic energy (E^e) along the lth normal coordinate (Q_l) evaluated at the ground state equilibrium geometry

$$I_{0 \rightarrow 1_l} \propto \frac{1}{\omega_l}\left(\frac{\partial E^e}{\partial Q_l}\right)_0^2$$

(1)

where ω_l is the frequency of the lth normal mode. The excited state gradients were obtained from the analytical (TDDFT) and numerical (RASSCF) derivatives of the excited state electronic energy (E^e) along the non-mass-weighted Cartesian coordinates.[29,35] The use of the STA for dye **1** is motivated by several things: (i) A single excited state is in resonance with the laser frequency. Therefore, contributions of other states can be neglected. (ii) The excited state in resonance (S_1) is strongly dipole-allowed. This indicates that only FC scattering is important. (iii) The first absorption band displays a large broadening and no resolved vibronic structure. This indicates that vibronic coupling effects should be small and that the relative RR intensities should show a weak dependence with respect to the excitation wavelength. Therefore, more sophisticated methods to simulate RR intensities (see e.g. refs 34, 35, 38−40) were not employed for the present application.

The relative RR intensities have been calculated with the functionals B3LYP, CAM-B3LYP, and M06-2X, as specified in section 2.1 and by means of SA2-RASSCF(16,3,3;7,2,7) on the B3LYP and the CAM-B3LYP equilibrium geometries. The vibrational frequencies were scaled by a factor of 0.97 for B3LYP and by 0.95 for CAM-B3LYP and M06-2X in order to correct for the lack of anharmonicity and the approximate treatment of electron correlation.[64,65]

3. RESULTS

3.1. Electronic Excited States Calculated at the TDDFT Level of Theory. The excitation energies, oscillator strengths, and main character of the wave function of the 10 lowest excited states calculated with the B3LYP, CAM-B3LYP, and M06-2X functionals are collected in Table 1. The MOs involved in the main configurations are depicted exemplarily for TD-CAM-B3LYP//CAM-B3LYP in Figure 4. The absorption spectra obtained for all of the functionals are depicted in solid lines in Figure 3.

The TD-B3LYP//B3LYP calculation predicts the S_1 bright state in chloroform at 1.69 eV (734 nm) with an oscillator strength of 1.02, see Table 1. This state involves a CT transition from the HOMO (147) orbital, mainly localized on the thiazole and the phenyl units, to the LUMO (148) orbital, localized on the anchoring group and the bridge (thia and thio). As is expected from a CT state, the excitation energy in the gas phase is blue-shifted (1.83 eV). The S_2 is another bright ($f = 0.58$) state at 2.57 eV, resulting from the CT of the π systems of the bridge and the donor to the bridge and the anchoring group. This state also blue-shifts in the gas phase by ca. 0.1 eV. The third excited singlet state at 3.01 eV features a less pronounced CT character, and therefore this state is only stabilized by 0.05 eV upon solvation. The following nearly degenerated states S_4 and S_5 at 3.49 and 3.51 eV refer to moderately intense CT states, while the higher excited states (S_6−S_{10}) are within 3.62 and 3.84 eV and show small oscillator strengths between 0.00 and 0.04. The CT states S_6, S_7, S_9, and S_{10} are stabilized by approximately 0.1 eV by going from the gas phase to chloroform. The experimental spectrum measured in chloroform is also depicted in Figure 3a, and a direct comparison with the solvated TD-B3LYP//B3LYP values shows that the obtained bands are significantly red-shifted by about 1 eV compared to the experimental spectrum. This disagreement can be associated with the tendency of hybrid functionals with a small amount of exact exchange, such as B3LYP, to underestimate CT states.[20,66−68]

The amount of Hartree−Fock exchange is increased in the long-range corrected CAM-B3LYP functional, depending on the electron−electron distance: for short range, it is 19% (B3LYP is 20%) and rises with an inverse error function to 65% for long-range interactions.[21] Since B3LYP is known to reproduce experimental equilibrium structures reasonably well, the B3LYP structure was first used to calculate the vertical spectrum of **1** with TD-CAM-B3LYP. As shown in Table 1, the solvated S_1 state (2.36 eV) is now in very good agreement with the first absorption band of the experimental spectrum at 2.39 eV. This very bright CT state is, similarly to TD-B3LYP//B3LYP, mainly due to the HOMO/LUMO transition. However, with CAM-B3LYP also the HOMO−1/LUMO transition exhibits a significant weight. The S_2 state is also shifted to higher energies with TD-CAM-B3LYP (3.44 eV) and can be assigned to the second absorption band of the experimental spectrum at 3.49 eV, see Figure 3a. The oscillator strength is drastically decreased in comparison to that predicted by TD-B3LYP. The third experimental band at 4.09 eV is mainly a superposition of two bright CT states from the bridge to the anchoring group (S_3 and S_4) and of one bright CT state from the bridge to the donor group (S_7). The remaining states (S_5, S_6, and S_8−S_{10}) are weakly absorbing and do not contribute to the absorption spectrum significantly. As in the TD-B3LYP//B3LYP calculation, solvation effects on the CT states lead to a red-shift of about 0.1 eV, with respect to the gas phase values.

Interestingly, the use of the CAM-B3LYP equilibrium structure (see TD-CAM-B3LYP//CAM-B3LYP results in Table 1) retains the order of states and leads to comparable intensities, but the excitation energies of the first four excited states are blue-shifted. Most significantly, the energy of S_1 increases by 0.22 eV, which makes the agreement with experimental values less good, see also Figure 3c. Applying the M06-2X functional, which possess the highest amount of exact exchange (54%), gives very similar results to the long-range corrected CAM-B3LYP functional (compare Figure 3c and d). Indeed, the S_1, S_2, and S_3 states keep the same order as the TD-CAM-B3LYP//CAM-B3LYP calculation, but the order of the higher excited states is only slightly altered.

In summary, the B3LYP functional fails to predict the excitation energies of **1**, while the long-range corrected CAM-B3LYP and M06-2X functionals show good performance on calculating the energetic positions of the UV absorption bands, provided solvation effects are included both in the geometry optimization and the calculation of excitation energies. In the particular case of the dye **1**, the first absorption band can be assigned to the S_1 state and the second band to the S_2, and the third band results from a superposition of three states: S_3, S_4, and S_7 in the case of CAM-B3LYP and S_3, S_5, and S_6 in case of M06-2X. The relative intensities of the second and third calculated bands are underestimated in comparison to the experiment, but the overall pattern of the spectrum is reasonably reproduced by the calculations. Interestingly, the combination of the B3LYP structure with the CAM-B3LYP functional (TD-CAM-B3LYP//B3LYP calculations) gives the best agreement with the experimental values, whereas the TD-CAM-B3LYP//CAM-B3LYP energies are blue-shifted with respect to the experimental spectrum. It should be mentioned that this comparison relies on the assumption that vertical excitation energies can be compared to the maximum of absorption. However, for related compounds it was shown (see e.g. refs 69, 70) that differences between the vertical excitation

Table 1. TDDFT Excitation Energies (ΔE), Oscillator Strengths (f), and Main Configurations of the Solvated (Chloroform) First 10 Singlet Excited States at TD-B3LYP//B3LYP, TD-CAM-B3LYP//B3LYP, TD-CAM-B3LYP//CAM-B3LYP, and TD-M06-2X//M06-2X Levels of Theory Obtained with the 6-31G(d,p) Basis Set[a]

state	TD-B3LYP//B3LYP				TD-CAM-B3LYP//B3LYP				TD-CAM-B3LYP//CAM-B3LYP				TD-M06-2X//M06-2X			
	ΔE/eV	f	character	c^2/%	ΔE/eV	f	character	c^2/%	ΔE/eV	f	character	c^2/%	ΔE/eV	f	character	c^2/%
S_1	1.69 (1.83)	1.02 (0.83)	147→148	100 (100)	2.36 (2.50)	1.60 (1.45)	147→148	77 (79)	2.58 (2.68)	1.52 (1.14)	147→148	71 (74)	2.55 (2.65)	1.44 (1.29)	147→148	78 (81)
							146→148	16 (14)			146→148	20 (17)			146→148	15 (12)
							147→149	4 (5)								
S_2	2.57 (2.69)	0.58 (0.64)	146→148	97 (94)	3.44 (3.54)	0.09 (0.13)	146→148	66 (71)	3.59 (3.67)	0.09 (0.14)	146→148	61 (67)	3.50 (3.58)	0.16 (0.22)	146→148	73 (78)
							147→148	13 (13)			147→148	16 (15)			147→148	13 (12)
							145→148	12 (10)			145→148	11 (10)				
S_3	3.01 (3.06)	0.19 (0.17)	147→149	91 (87)	3.86 (3.92)	0.17 (0.16)	147→149	68 (72)	3.97 (4.02)	0.22 (0.20)	147→149	62 (67)	3.88 (3.93)	0.29 (0.24)	147→149	72 (75)
			145→148	5 (9)			146→149	10 (8)			146→149	10 (9)			147→151	11 (11)
							147→148	8 (6)			147→148	11 (8)				
							147→151	7 (8)			147→151	10 (11)				
S_4	3.49 (3.58)	0.05 (0.05)	145→148	44 (50)	4.16 (4.24)	0.33 (0.26)	145→148	45 (56)	4.30 (4.37)	0.34 (0.27)	145→148	30 (45)	4.23 (4.24)	0.04 (0.03)	147→150	85 (85)
			144→148	44 (29)			143→148	15 (11)			143→148	18 (17)				
			146→149	3 (9)			140→148	13 (12)			140→148	10 (11)				
							147→151	8 (5)			147→151	10 (8)				
							146→149	6 (6)			147→150	10 (-)				
							146→148	6 (5)			146→149	8 (9)				
S_5	3.51 (3.59)	0.07 (0.10)	145→148	44 (48)	4.27 (4.29)	0.03 (0.02)	147→150	74 (72)	4.31 (4.32)	0.04 (0.03)	147→150	71 (80)	4.31 (4.39)	0.30 (0.25)	145→148	39 (50)
			144→148	44 (27)											143→148	19 (15)
			146→149	3 (9)											146→149	11 (10)
															147→151	11 (9)
S_6	3.62 (3.71)	0.04 (0.01)	143→148	90 (90)	4.35 (4.43)	0.04 (0.04)	139→148	83 (79)	4.45 (4.52)	0.03 (0.03)	139→148	79 (76)	4.45 (4.47)	0.33 (0.26)	147→152	86 (85)
							140→148	8 (8)			140→148	12 (10)			146→152	9 (9)
S_7	3.67 (3.80)	0.01 (0.00)	142→148	53 (68)	4.52 (4.53)	0.35 (0.29)	147→152	78 (79)	4.54 (4.57)	0.37 (0.29)	147→152	83 (83)	4.47 (4.53)	0.02 (0.01)	139→148	66 (59)
			147→150	22 (14)			146→152	12 (12)			146→152	11 (10)			140→148	19 (29)
			141→148	11 (11)												
			144→148	10 (-)												
S_8	3.74 (3.72)	0.02 (0.02)	147→150	70 (70)	4.63 (4.66)	0.11 (0.08)	147→151	42 (41)	4.72 (4.75)	0.05 (0.03)	147→151	37 (32)	4.64 (4.67)	0.03 (0.03)	147→151	39 (37)
			142→148	24 (6)			146→149	22 (20)			146→149	21 (16)			146→149	21 (16)
			144→148	- (18)			145→148	8 (7)			147→153	- (9)			139→148	10 (19)
							139→148	5 (7)							145→148	9 (8)
S_9	3.82 (3.90)	0.01 (0.02)	140→148	43 (49)	4.65 (4.62)	0.00 (0.00)	138→148	72 (74)	4.73 (4.71)	0.00 (0.00)	138→148	55 (66)	4.73 (4.73)	0.08 (0.07)	147→153	63 (60)
			141→148	22 (7)			138→149	10 (13)			136→148	21 (9)			146→150	9 (9)
			146→149	13 (15)							138→149	- (10)				
			139→148	10 (12)												
S_{10}	3.84 (3.93)	0.00 (0.02)	141→148	58 (62)	4.71 (4.71)	0.03 (0.03)	147→153	42 (43)	4.78 (4.77)	0.05 (0.05)	147→153	54 (44)	4.78 (4.75)	0.00 (0.00)	138→148	56 (51)
			140→148	20 (6)			141→148	10 (7)			146→150	9 (7)			138→149	13 (13)
			142→148	11 (7)			146→150	8 (8)							136→148	12 (15)
			147→152	- (15)			147→150	6 (6)								
							142→149	5 (5)								

[a]All values in parentheses refer to the respective gas phase calculations.
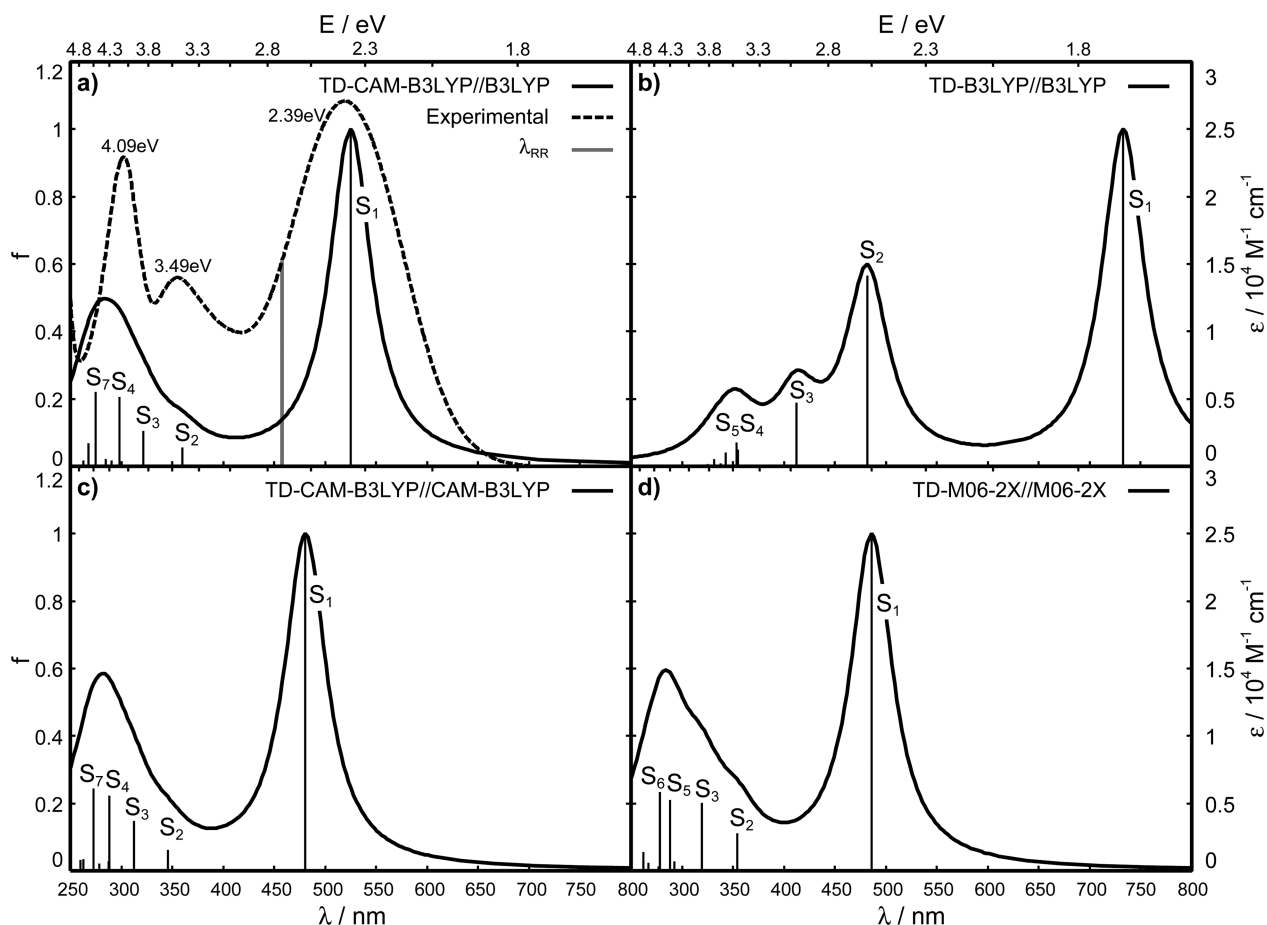
Figure 3. UV/vis absorption spectra of **1** (solid lines) in chloroform calculated as indicated. The experimental absorption spectrum recorded in chloroform (dashed lines) is also plotted in a. The absorption maxima correspond to 2.39 eV ($\varepsilon = 27\,050$ M^{-1} cm^{-1}), 3.49 eV ($\varepsilon = 14\,050$ M^{-1} cm^{-1}), and 4.09 eV ($\varepsilon = 22\,950$ M^{-1} cm^{-1}). The excitation wavelength of 2.70 eV (458 nm) used in the RR measurement is plotted in gray.
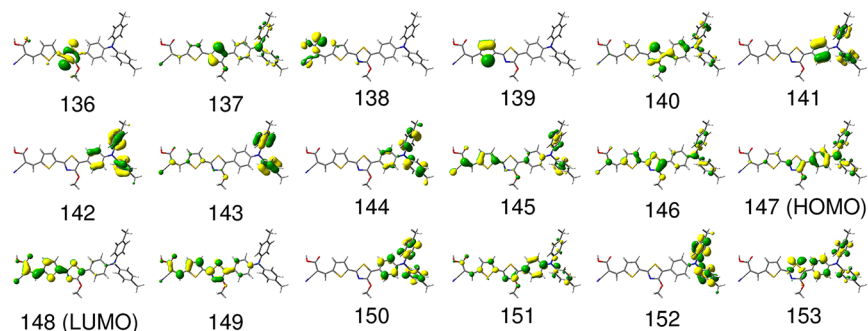

Figure 4. Molecular orbitals involved in the 10 lowest singlet excited states of **1** at the TD-CAM-B3LYP//CAM-B3LYP level of theory.

energies and the maximum of absorption can be as large as 0.3 eV. Such a shift is comparable to the obtained accuracy of the TDDFT calculations. Therefore, the comparison of TDDFT excitation energies with experimental absorption spectra cannot provide an unambiguous identification of which ground state geometry is best.

From the comparison of gas phase and solvated values, we see that the solvent influences the excitation energies of the low-lying singlet excited states in a different way. Note that the geometries employed in all of the calculations (gas phase and IEFPCM) are always the solvated ones, in order to separate the solvation effect on the energies from the solvation effect on the geometries (not considered here due to its small effect). In

general, the excitation energies of CT states red-shift by about 0.1 eV from gas to chloroform. The exact amount obtained with each functional is though not identical: The solvent stabilization for S_1 is 0.14 eV with TD-B3LYP//B3LYP and TD-CAM-B3LYP//B3LYP and 0.10 eV with TD-CAM-B3LYP//CAM-B3LYP and TD-M06-2X//M06-2X. Comparable shifts have been determined for the CT states contributing to the second (0.08 to 0.12 eV) and third absorption band (0.05 to 0.08 eV), while the states S_7 with TD-CAM-B3LYP//B3LYP and TD-CAM-B3LYP//CAM-B3LYP and S_6 with TD-M06-2X//M06-2X, respectively, are almost unaffected (0.01 to 0.03 eV) by solvent interactions.

Table 2. MS-RASPT2 Excitation Energies (ΔE), Oscillator Strengths (f), and Wavefunctions for the Partitions (30,2,2;14,2,11), (16,2,2;7,2,7), (16,3,3;7,2,7), and (16,4,4;7,2,7) for the S_1 State in the B3LYP and CAM-B3LYP Equilibrium Structures[a]

		B3LYP geometry				CAM-B3LYP geometry		
ΔE/eV		f	character	c^2/%	ΔE/eV		f	character	c^2/%
				RASPT2 (30,2,2;14,2,11) (CSFs: 61131)					
2.45	(2.35)	1.34	147 → 148	73	2.62	(2.52)	1.27	147 → 148	75
				RASPT2 (16,2,2;7,2,7) (CSFs: 6947)					
2.57	(2.47)	1.06	147 → 148	78	2.74	(2.64)	1.02	147 → 148	79
				RASPT2 (16,3,3;7,2,7) (CSFs: 96323)					
2.42	(2.32)	1.26	147 → 148	72	2.61	(2.51)	1.15	147 → 148	75
				RASPT2 (16,4,4;7,2,7) (CSFs: 725875)					
2.35	(2.25)	1.41	147 → 148	62	2.47	(2.37)	1.31	147 → 148	65
			147 → 149	7				147 → 149	4
								144 → 148	4

[a]All values in parentheses refer to the approximated excitation energies in chloroform taking a solvent stabilization of 0.1 eV into account (see TDDFT results of Table 1).

3.2. Electronic Excited States Calculated at the MS-RASPT2 Level of Theory.

The MS-RASPT2/RASSCF study focuses exclusively on the first CT state (S_1), which is the one responsible for many of the applications of **1** as a dye. Due to the computational cost in using a PCM model with multiconfigurational methods, the calculations were performed only in the gas phase—although using both the B3LYP and the CAM-B3LYP solvated equilibrium geometries. The corresponding vertical excitation energies, oscillator strengths, and associated wave functions of the CT transitions are collected in Table 2. The orbital numbering corresponds to that of Figure 2. First, the properties of the S_1 state obtained with the B3LYP equilibrium structure shall be reported, followed by the results obtained on the CAM-B3LYP structure. All four RASSCF partitions, (30,2,2;14,2,11), (16,2,2;7,2,7), (16,3,3;7,2,7), and (16,4,4;7,2,7), were employed.

All levels of theory predict the S_1 state as a very bright CT state, mainly described by the HOMO(147)/LUMO(148) transition. The large MS-RASPT2 (30,2,2;14,2,11) calculation predicts an excitation energy of 2.45 eV, with an oscillator strength of 1.34. The HOMO−LUMO transition dominates with a weight of 73% while examination of the remaining wave function coefficients shows only marginal influence of the π-system of ph2 and ph3. Using the smaller (16,2,2;7,2,7) partition, where these orbitals with negligible contributions to the wave function are removed and including only SD excitations, an increase of the excitation energy of 0.12 eV, an increase of the weight of the HOMO/LUMO transition (78%), and a decrease of the oscillator strength (1.06) are obtained. The increase of the excitation level up to triples or quadruples lowers the energy to 2.42 and 2.35 eV, respectively, whereas the oscillator strength increases to 1.26 and 1.41. It is interesting to note the associated computational cost of these calculations: while the smaller (16,2,2;7,2,7) partition involves 10 times less CSFs (and substantial less amount of memory) than (30,2,2;14,2,11) at the same level of excitation, the inclusion of triple and quadruples excitations in (16,2,2;7,2,7) again increases the number of CSFs by 1 and 2 orders of magnitude, at the expense of decreasing the energy by ca. 0.1 and 0.2 eV, respectively. Noticeable is also the decrease of the HOMO/LUMO transition weight in the MS-RASPT2 (16,4,4;7,2,7) calculation, while the weight of the 147 → 149 transition is increased. In passing, we note that this transition was also observed in the S_1 state predicted by TD-CAM-B3LYP//B3LYP, see Table 1.

Using the optimized CAM-B3LYP geometry, MS-RASPT2 (30,2,2;14,2,11) yields an excitation energy of 2.62 eV, and the composition of the S_1 and oscillator strength (1.27) resembles that obtained with the B3LYP geometry. Again, reducing the active space to (16,2,2;7,2,7) increases the excitation energy (2.74 eV) and decreases the oscillator strength (1.02). The inclusion of triples and quadruples stabilizes the S_1 to 2.61 and 2.47 eV, respectively. As with using the B3LYP geometry, a more pronounced multiconfigurational character of the S_1 state is obtained including Q excitations. Note that a similar wave function composition was also observed in the TD-CAM-B3LYP//CAM-B3LYP and TD-M06-2X//M06-2X calculations, see Table 1.

While the trends obtained with the different RASSCF partitions are similar with both geometries, the specific excitation energies are strongly dependent on the ground state geometry. The RASPT2 energy based on the CAM-B3LYP geometry fluctuates up to 0.27 eV, depending on the partition, while the variation within the B3LYP geometry is, with 0.22 eV, slightly smaller. In order to discuss which of both geometries performs better and which partition is more adequate, and in the light of the experimental values available, it is necessary to take solvent effects into account. From the previous TDDFT calculations (see section 3.1), the effect of chloroform on the absorption energy of the CT state S_1 can be estimated as a red-shift of ca. 0.1 eV. The result of subtracting this correction to the gas phase values is shown in parentheses in Table 2. From these values, it can be seen that the best agreement with the experimental value of 2.39 eV is obtained with the (30,2,2;14,2,11) calculation in combination with the B3LYP geometry (2.35 eV) and the (16,4,4;7,2,7) calculation in combination with the CAM-B3LYP geometry (2.37 eV). Acceptable errors (within 0.1−0.2 eV) are nevertheless obtained with all the partitions regardless of the geometry, except the (16,2,2;7,2,7) and the CAM-B3LYP geometry (2.64 eV). It seems that the inclusion of SD is in general not sufficient to account for enough dynamical correlation to provide good energies, as found by Gagliardi and co-workers.[17] The fact that the inclusion of T and Q systematically decreases the energy with respect to SD indicates that such a level of excitation might be necessary. In combination with the CAM-B3LYP geometry, the obtained energy with SDTQ is the best; in combination with the B3LYP structure, the good value obtained with SDT is again undershot by including Q.

In conclusion, similarly to the TDDFT results the RASPT2 calculations cannot give a definite answer about which equilibrium geometry is best used in combination with RASPT2/RASSCF. In that respect, RR provides a unique framework to assess further the quality of the electronic structures and corresponding gradients. Before discussing RR spectra, we shall analyze the geometrical features obtained with both B3LYP and CAM-B3LYP functionals.

3.3. Electronic Ground State Geometries. As predicted in sections 3.1 and 3.2, the ground state geometry can have a substantial impact on the excitation energies. This is especially true in the case of the S_1 of **1**, but changes are also obtained in the vertical energies of the S_2, S_3, and S_4 states. In order to interpret the origin of these changes, two geometrical parameters were investigated in more detail, namely the dihedral angle δ (Figure 1) and the bond length alternation (BLA) index.[36,71] The BLA index is defined as the difference between the average length of carbon−carbon single bonds and double bonds, and it can be applied to polyenes, conjugated π systems, or push−pull chromophores such as **1**. A positive BLA index is correlated to a neutral form, a negative value to a zwitterionic form, and a zero value to a delocalized system. For **1**, the BLA index was calculated along the conjugated path joining the triphenylamine moiety (donor group) to the cyano group (anchoring group; see Figure S1 and Table S1 of the Supporting Information).

The comparison of the B3LYP and CAM-B3LYP equilibrium structures reveals a difference in the dihedral angle δ, which takes values of −14 and −19° at the B3LYP and CAM-B3LYP geometries, respectively. These changes affect the conjugation between the donor group and the bridge and therefore could modify the excitation energies. In order to explicitly study the influence of δ on the S_1 excitation energies, potential energy curves (PEC) of S_0 and S_1 states along δ were calculated starting from the B3LYP and CAM-B3LYP equilibrium structures and leaving the other coordinates frozen. The PECs were investigated in the interval [−30°;30°] with a step size of 0.5° using TD-CAM-B3LYP in the presence of chloroform. As can be seen from Figure 5, the B3LYP and CAM-B3LYP minima for the S_0 state are associated with a twisted structure, whereas the minima of the S_1 are nearly planar, which can be understood from the double bonding character of the LUMO (see Figure 4) between the ph1 and thia units. Moreover, Figure 5 shows that the PECs obtained with both geometries display a very similar shape. In particular, the 0.22 eV energy difference between the S_0 and the S_1 is almost independent from the dihedral angle δ with both geometries; i.e., both curves run mostly parallel. This indicates that the difference in the S_1 excitation energy obtained with B3LYP and CAM-B3LYP geometries is not a consequence of the different torsion angle but must be associated with other geometrical changes along the conjugated path.

The calculated BLA indexes for **1** are all positive, corresponding to a neutral form. The BLA index obtained with CAM-B3LYP (0.0335 Å) is larger than that calculated with B3LYP (0.0203 Å). Hence, the geometry obtained with CAM-B3LYP is more localized than the B3LYP geometry. This fact allows for an interpretation of the difference in excitation energy for the S_1 state. The virtual MO 148 involved in the S_1 excitation (Figure 4, see also Figure 2) shows a bonding character on the single bonds and an antibonding character on the double bonds, i.e., photoexcitation leads to a more zwitterionic form (see Table S1 of the Supporting Information
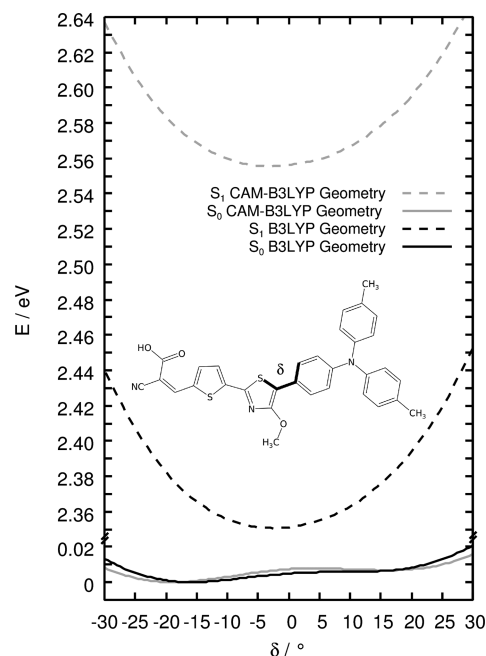

Figure 5. Potential energy curves of the S_0 and S_1 states calculated with CAM-B3LYP along the dihedral angle δ starting from the optimized B3LYP (black) and CAM-B3LYP (gray) geometries.

and e.g. refs 35, 36). Therefore, since the single and double bonds of the CAM-B3LYP equilibrium structure are more localized than those of the B3LYP geometry, the MO 148 is stabilized (0.16 eV) when going from the CAM-B3LYP to the B3LYP geometry, and as a consequence, the excitation energy for a transition to the MO 148 is higher in TD-CAM-B3LYP// CAM-B3LYP than in TD-CAM-B3LYP//B3LYP. In passing, we note that the BLA index for the M06-2X geometry (0.0332 Å) is similar to that of CAM-B3LYP, and hence, a similar excitation energy for S_1 is obtained. Analogous reasonings can explain the decrease observed in the excitation energies of S_2, S_3, and S_4 states, when going from the CAM-B3LYP to the B3LYP structures.

In conclusion, the differences in the excitation energies obtained with the different optimized structures can be attributed to the changes in the bond length alternation of single and double bonds.

3.4. Resonance Raman Spectra. A non-negligible effect of the ground state structure has been observed on the excitation energies. However, it is not clear which method is more suited to describe the ground state geometry of compound **1** and consequently of structurally related dyes. Therefore, the calculation of RR spectra in resonance with the first absorption band is used to obtain additional information on the quality of ground and excited state structures.

Figure 6 shows the RR spectra calculated with the different methods, compared to the experimental one recorded for an excitation wavelength of 2.7 eV (458 nm). For completeness, the RR spectra are not only calculated with the B3LYP and CAM-B3LYP geometries using TD-CAM-B3LYP and RASSCF procedures but also employing the TD-B3LYP//B3LYP and TD-M06-2X//M06-2X protocols. The calculated vibrational modes and corresponding assignments are in Tables 3, 4, and 5.

The spectrum simulated with TD-B3LYP//B3LYP (Figure 6a) allows for a rough assignment of the vibrational bands (Table 3), but the relative intensities of the peaks are very
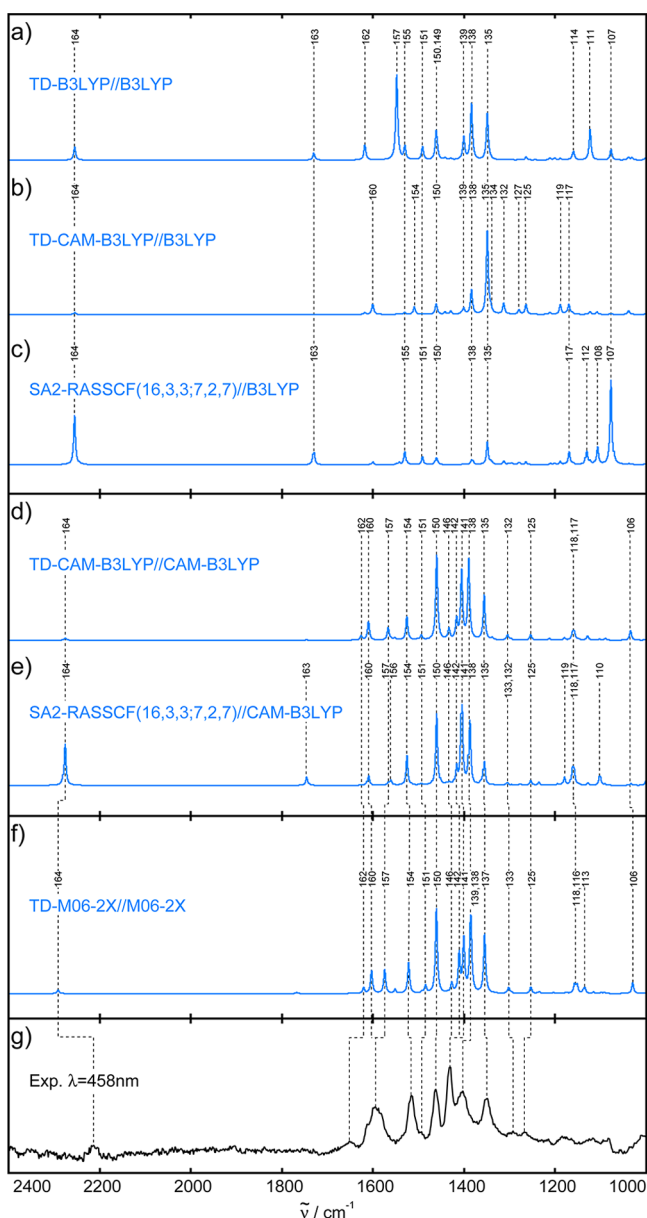
Figure 6. RR spectra of **1** in resonance with the first absorption band. The notation F2//F1 is used, in which F1 represents the XC functional employed for the ground state properties and F2 is the method used for the excited state gradients calculation.

Table 3. Assignment of the Vibrational Frequencies (cm^{-1}) and Calculated Relative RR Intensities ($I_{rel.}$) Using the B3LYP Optimized Structure^a

mode	$\tilde{\nu}$/cm^{-1}	$I_{rel.}$ B3LYP	$I_{rel.}$ CAM−B3LYP	$I_{rel.}$ RASSCF	assignment
107	1077.5	0.12	0.01	0.36	bridge, donor
108	1108.4	<0.01	0.03	0.07	bridge, acceptor
111	1123.5	0.36	0.03	0.01	acceptor, bridge
112	1130.8	<0.01	<0.01	0.06	donor
114	1159.8	0.1	<0.01	<0.01	donor
117	1170	<0.01	0.12	0.05	bridge
119	1188.8	0.02	0.12	0.01	donor
125	1264.1	0.04	0.12	0.01	bridge, donor
127	1279.7	<0.01	0.05	0.01	donor
132	1313.1	0.01	0.13	0.02	donor
134	1341.5	0.01	0.06	0.01	acceptor, bridge
135	1349.1	0.54	1	0.1	acceptor, bridge
138	1383.8	0.65	0.29	0.02	bridge, donor
139	1400.7	0.26	0.07	<0.01	acceptor, bridge
149	1458.8	0.06	0.01	<0.01	bridge
150	1461.3	0.31	0.12	0.03	bridge
151	1491.2	0.16	<0.01	0.03	bridge, donor
154	1509.4	0.01	0.09	<0.01	donor, bridge, acceptor
155	1530.1	0.15	0.02	0.06	bridge, donor
157	1547.9	1	<0.01	<0.01	acceptor, bridge
160	1600.5	<0.01	0.13	0.01	donor
162	1617.8	0.18	0.02	<0.01	donor
163	1729.9	0.08	<0.01	0.05	acceptor, bridge
164	2254.8	0.16	0.02	0.21	acceptor, bridge

^{a}The theoretical frequencies were scaled by a factor of 0.97.

Table 4. Assignment of the Vibrational Frequencies (cm^{-1}) and Calculated Relative RR Intensities ($I_{rel.}$) Using the CAM-B3LYP Optimized Structure^a

mode	$\tilde{\nu}_{(Cal.)}$/cm^{-1}	$\tilde{\nu}_{(Exp.)}$/cm^{-1}	$I_{rel.}$ CAM−B3LYP	$I_{rel.}$ RASSCF	assignment
106	1034.6	−	0.11	0.02	bridge, acceptor
110	1102.9	−	0.01	0.12	bridge, acceptor
117	1158.5	−	0.07	0.16	bridge
118	1162	−	0.08	0.2	donor
119	1179.8	−	0.03	0.1	donor
125	1253.7	−	0.07	0.07	bridge
132	1304.5	−	0.05	0.02	donor
135	1356	1351	0.53	0.3	acceptor, bridge
138	1389.8	1403	0.93	0.81	bridge
141	1405.4	1431	0.8	1	bridge, acceptor
142	1416.5	1431	0.23	0.22	bridge, donor
146	1433.2	1431	0.12	0.03	bridge, acceptor
150	1460.2	1462	1	0.91	bridge
151	1493.7	1494	0.05	0.02	donor
154	1525.7	1516	0.28	0.38	bridge
156	1560.8	−	0.01	0.06	donor, bridge, acceptor
157	1566.7	1595	0.14	0.03	acceptor
160	1609.9	1595	0.22	0.12	donor
162	1626	1652	0.05	<0.01	donor
163	1745.4	−	<0.01	0.11	acceptor
164	2275.8	2213	0.03	0.53	acceptor

^{a}The theoretical frequencies were scaled by a factor of 0.95.

inaccurate, in comparison to the experimental spectrum (Figure 6g). This could indicate a wrong estimation of the excited state gradients by B3LYP, and it might also be related to the strong underestimation of the S_1 excitation energy by this functional (recall Table 1). Since energies of CT states can be corrected with CAM-B3LYP, the RR spectrum was also calculated using the TD-CAM-B3LYP//B3LYP method. Recently, this approach has provided improved RR spectra in comparison to the TD-B3LYP//B3LYP one in the case of *o*-nitrophenol.[29] However, as shown in Figure 6b, the obtained results for **1** are very poor. Also the RR intensity pattern at the SA2-RASSCF(16,3,3;7,2,7)//B3LYP level of theory is extremely bad (Figure 6c). Here, the (16,3,3;7,2,7) partition including up to T excitations has been chosen as a reasonable compromise between accuracy and computational cost (cf. Table 2). The results obtained with the latter two methods indicate that the

Table 5. Assignment of the Vibrational Frequencies (cm⁻¹) and Calculated Relative RR Intensities ($I_{rel.}$) Using the M06-2X Optimized Structure[a]

mode	$\tilde{\nu}_{(Cal.)}/cm^{-1}$	$\tilde{\nu}_{(Exp.)}/cm^{-1}$	$I_{rel.}$ M06-2X	assignment
106	1029.9	–	0.13	bridge, acceptor
113	1135.2	–	0.07	acceptor, bridge
116	1151.9	–	0.09	donor
118	1157.8	–	0.09	bridge
125	1253.4	–	0.08	bridge, donor
133	1302.3	–	0.07	donor
137	1355.1	1351	0.68	bridge
138	1384.8	1403	0.58	acceptor
139	1386.5	1403	0.42	acceptor
141	1400.8	1431	0.62	bridge, acceptor
142	1410.8	1431	0.46	bridge, donor
146	1427.1	1431	0.11	bridge, acceptor
150	1460.7	1462	1.00	bridge
151	1484.6	1494	0.08	donor
154	1521.7	1516	0.36	bridge, donor
157	1574.2	1595	0.27	acceptor
160	1603.2	1595	0.27	donor
162	1620.4	1652	0.07	donor
164	2290.8	2213	0.04	acceptor

[a]The theoretical frequencies were scaled by a factor of 0.95.

inaccuracies in the RR spectra are more likely to be associated with inaccuracies of the ground state geometry and associated vibrational normal coordinates rather than with excited state energies and gradients.

Indeed, the RR spectrum calculated with the TD-CAM-B3LYP//CAM-B3LYP method (Figure 6d) presents a much better agreement with experimental values (Figure 6g). Almost all calculated vibrational modes (see Table 4) were assigned to the experiment; merely the assignment of the modes between 1000 and 1300 cm⁻¹ was not feasible due to the pronounced experimental noise. The frequencies of the modes in the range between 1300 and 1700 cm⁻¹ are in good agreement with the experiment with a typical mean absolute deviation of 15 cm⁻¹. The RR spectrum obtained with the TD-M06-2X//M06-2X method is very similar to the TD-CAM-B3LYP//CAM-B3LYP spectrum (Figure 6f and Table 5), even if some differences are found for the relative intensities of the modes 135, 142, 154, and 157. The remaining disagreements with the experimental spectrum can be attributed to limitations of the XC functionals, of the description of the solvent, as well as of the STA, which only makes use of excited state gradients at the FC point. However, these inaccuracies are small enough to allow an assessment of the calculated geometries and gradients.

Almost all intense RR normal modes in the CAM-B3LYP and the M06-2X equilibrium structures are centered either at the bridge or the anchoring group, see Tables 4 and 5. Only the less intense modes 118, 119, and 132 (CAM-B3LYP structure) or rather 116 and 133 (M06-2X structure) as well as 151, 160, and 162 are located at the donor group. This is consistent with the observed CT nature of the S_1 state discussed in sections 3.1 and 3.2. The obtained intensity patterns at TD-CAM-B3LYP//CAM-B3LYP (Figure 6d) and TD-M06-2X//M06-2X (Figure 6f) are very similar. However, SA2-RASSCF(16,3,3;7,2,7)//CAM-B3LYP (Figure 6e) features some minor variations in the intensities in the region between 1500 and 1600 cm⁻¹, such as a substantially increased intensity of mode 164, which is related to the stretching of the cyano group.

These results confirm that both ground and excited state properties of **1** are better described with the long-range corrected CAM-B3LYP (or the M06-2X) functional and should be preferred in calculating ground and excited state geometries for push−pull chromophores similar or related to the dye **1**. The adequacy of the CAM-B3LYP ground state structure is also corroborated by the SA2-RASSCF(16,3,3;7,2,7)//CAM-B3LYP RR spectrum (Figure 6e), which presents a similar pattern to that of the spectrum obtained with the CAM-B3LYP//CAM-B3LYP calculation. These results are very encouraging and constitute a first application of the RASSCF methodology to the simulation of RR intensities.

4. CONCLUSIONS

In this paper, the excitation energies and gradients in the ground and the first excited state of an organic push−pull chromophore have been assessed with TDDFT and RASPT2/RASSCF methods. To this aim, equilibrium geometries and UV/vis absorption and RR spectra are calculated for the 4-methoxy-1,3-thiazole donor−acceptor dye (**1**). Substantial effort was put into characterizing the bright CT state (S_1) that is located at a remarkably low excitation energy for this family of push−pull chromophores.

In order to compare with available absorption and RR spectra obtained in chloroform, first the solvated equilibrium geometries were calculated using the global hybrid functionals B3LYP and M06-2X and the long-range corrected CAM-B3LYP functional. These geometries and the same functionals were employed within TDDFT to calculate the vertical energies of the low-lying excited states in the presence of a polarized continuum to model the solution. It was found that not only does the amount of exact exchange in the functional have a strong influence on the accuracy of the excitation energies but the latter also markedly depend on the equilibrium structure employed. Up to 0.2 eV differences can be found when going from the B3LYP to the CAM-B3LYP geometry. These energy differences can be rationalized analyzing the variations of the torsion angle of the carbon−carbon bond joining the bridge and the donor group (dihedral angle δ) as well as the extent of localization of the single and double bonds, measured by the BLA index. While energy profiles along δ showed that torsion is of minor importance to the S_1 excitation energy, it was found that a more pronounced amount of exact exchange leads to larger BLA indexes, i.e., a more localized nature of the single and double bonds, thus increasing the excitation energies. In this way, changes of the BLA index in the ground state structures could be correlated to differences in excitation energy. From the three functionals investigated, B3LYP fails to predict the excitation energies of **1**, due to its intrinsic problems in describing CT states, while CAM-B3LYP and M06-2X functionals deliver good agreement with the experiment, provided solvation effects are included. As estimated from TDDFT, the solvent red-shifts the excitation energies by about 0.1 eV. The best estimation of the S_1 energy, with respect to the experimental data, was found using TD-CAM-B3LYP//B3LYP.

Using the B3LYP and CAM-B3LYP geometries, the position of the S_1 state was also investigated by means of MS-RASPT2/RASSCF calculations. Four different partitions, changing the active space and the level of excitation, were employed: (30,2,2;14,2,11), (16,2,2;7,2,7), (16,3,3;7,2,7), and (16,4,4;7,2,7). All of them contain only the HOMO and LUMO orbitals in the RAS2, while a different number of ligand orbitals, holes, and particles are allowed within the RAS1 and

RAS3 subspaces. As with TDDFT, the MS-RASPT2 calculations also showed a dependency of the S_1 excitation energy on the equilibrium structure and the partition employed. Although in some cases errors can be considered acceptable (0.1−0.2 eV), it seems that in this particular case, where the RAS2 is reduced to HOMO−LUMO, the inclusion of at least T excitations is necessary to achieve good excitation energies— similar to the results of Gagliardi et al in ref 17. The best agreement in the first absorption band was obtained with the CAM-B3LYP geometry and the (16,4,4;7,2,7) partition, while the excitation energy obtained with the B3LYP structure and the same level of excitation (SDTQ) is underestimated. The large (30,2,2;14,2,11) partition also provides a good estimation of the excitation energy for the present dye in combination with the B3LYP geometry. However, from the computational point of view, the (30,2,2;14,2,11) partition is associated with an enormous cost in the MS-RASPT2 procedure, arising from the first-order perturbative wave function.

Since MS-RASPT2/RASSCF calculations cannot provide a clear-cut answer on which ground state geometry is more adequate, RR intensity patterns were calculated, paying special attention to the B3LYP and CAM-B3LYP structures. TDDFT and RASSCF gradients using the compromised (16,3,3;7,2,7) partition were employed. To our knowledge, this is the first time that RASSCF gradients have been used to compute RR intensities. The results clearly evidence that only the RR spectra using the CAM-B3LYP (and M06-2X) equilibrium structure show an excellent agreement with experimental values, which allows an unambiguous assignment of the normal modes. Both CAM-B3LYP and RASSCF excited state gradients and energies in combination with CAM-B3LYP ground state gradients are appropriate to describe the CT state of this push−pull chromophore. Particularly encouraging is the agreement on RR intensities based on RASSCF, since despite the computational cost, it paves the way to employing multiconfigurational gradients in situations where conventional TDDFT calculations might fail completely to provide accurate results.

ASSOCIATED CONTENT

Supporting Information

Bond lengths of the ground state equilibrium structures (B3LYP, CAM-B3LYP, and M06-2X), excited state geometries calculated from the excited state gradients assuming displaced harmonic oscillators (B3LYP//B3LYP, CAM-B3LYP//CAM-B3LYP, and M06-2X//M06-2X) and BLA indexes are provided in Figure S1 and Table S1. This material is available free of charge via the Internet at http://pubs.acs.org.

AUTHOR INFORMATION

Corresponding Author
*E-mail: leticia.gonzalez@univie.ac.at.

Notes
The authors declare no competing financial interest.

ACKNOWLEDGMENTS

REFERENCES

(1) Lynch, B. J.; Truhlar, D. G. *J. Phys. Chem. A* **2001**, *105*, 2936−2941.
(2) Budyka, M. F.; Zyubina, T. S.; Zarkadis, A. K. *J. Mol. Struct.: THEOCHEM* **2002**, *594*, 113−125.
(3) Chai, J.-D.; Head-Gordon, M. *J. Chem. Phys.* **2008**, *128*, 084106-1−084106-15.
(4) Georgieva, I.; Aquino, A. J. A.; Trendafilova, N.; Santos, P. S.; Lischka, H. *Inorg. Chem.* **2010**, *49*, 1634−1646.
(5) Cramer, C. J.; Truhlar, D. G. *Chem. Rev.* **1999**, *99*, 2161−2200.
(6) Tomasi, J.; Mennucci, B.; Cammi, R. *Chem. Rev.* **2005**, *105*, 2999−3093.
(7) González, L.; Escudero, D.; Serrano-Andrés, L. *Chem. Phys. Chem.* **2012**, *13*, 28−51.
(8) Magyar, R. J.; Tretiak, S. *J. Chem. Theory Comput.* **2007**, *3*, 976−987.
(9) Pastore, M.; Mosconi, E.; De Angelis, F.; Grätzel, M. *J. Phys. Chem. C* **2010**, *114*, 7205−7212.
(10) Faber, C.; Duchemin, I.; Deutsch, T.; Attaccalite, C.; Olevano, V.; Blase, X. *J. Mater. Sci.* **2012**, *47*, 7472−7481.
(11) Malmqvist, P.-Å.; Pierloot, K.; Shahi, A. R. M.; Cramer, C. J.; Gagliardi, L. *J. Chem. Phys.* **2008**, *128*, 204109-10−204109-1.
(12) Manni, G. L.; Aquilante, F.; Gagliardi, L. *J. Chem. Phys.* **2011**, *134*, 034114−1−034114−5.
(13) Malmqvist, P.-Å.; Rendell, A.; Roos, B. O. *J. Phys. Chem.* **1990**, *94*, 5477−5482.
(14) Olsen, J.; Roos, B. O.; Jørgensen, P.; Jensen, H. J. A. *J. Chem. Phys.* **1988**, *89*, 2185−2192.
(15) Finley, J.; Malmqvist, P.-A.; Roos, B. O.; Serrano-Andrés, L. *Chem. Phys. Lett.* **1998**, *288*, 299−306.
(16) Roos, B. O. In *Ab Initio Methods in Quantum Chemistry II*; Wiley-VCH: Chichester, U. K., 1987.
(17) Sauri, V.; Serrano-Andres, L.; Shahi, A. R. M.; Gagliardi, L.; Vancoillie, S.; Pierloot, K. *J. Chem. Theory Comput.* **2011**, *7*, 153−168.
(18) Kupfer, S.; Pérez-Hernández, G.; González, L. *Theor. Chem. Acc.* **2012**, *131*, 1295.
(19) Runge, E.; Gross, E. K. U. *Phys. Rev. Lett.* **1984**, *52*, 997−1000.
(20) Dreuw, A.; Head-Gordon, M. *J. Am. Chem. Soc.* **2004**, *126*, 4007−4016.
(21) Yanai, T.; Tew, D. P.; Handy, N. C. *Chem. Phys. Lett.* **2004**, *393*, 51−57.
(22) Becke, A. D. *J. Chem. Phys.* **1993**, *98*, 1372−1377.
(23) Zhao, Y.; Truhlar, D. G. *Theor. Chem. Acc.* **2008**, *120*, 215−241.
(24) Lange, A. W.; Rohrdanz, M. A.; Herbert, J. M. *J. Phys. Chem. B* **2008**, *112*, 6304−6308.
(25) Jacquemin, D.; Wathelet, V.; Perpète, E. A.; Adamo, C. *J. Chem. Theory Comput.* **2009**, *5*, 2420−2435.
(26) Jacquemin, D.; Mennucci, B.; Adamo, C. *Phys. Chem. Chem. Phys.* **2011**, *13*, 16987−16998.
(27) Aquino, A. J.; Nachtigallova, D.; Hobza, P.; Truhlar, D. G.; Hättig, C.; Lischka, H. *J. Comput. Chem.* **2011**, *32*, 1217−1227.
(28) Steinmann, S. N.; Piemontesi, C.; Delachat, A.; Corminboeuf, C. *J. Chem. Theory Comput.* **2012**, *8*, 1629−1640.
(29) Guthmuller, J. *J. Chem. Theory Comput.* **2011**, *7*, 1082−1089.
(30) Jang, S.; Jin, S. I.; Park, C. R. *Bull. Korean Chem. Soc.* **2007**, *28*, 2343−2353.
(31) Bahers, T. L.; Pauporté, T.; Scalmani, G.; Adamo, C.; Ciofini, I. *Phys. Chem. Chem. Phys.* **2009**, *11*, 11276−11284.
(32) Menzel, R.; Ogermann, D.; Kupfer, S.; Weiß, D.; Görls, H.; Kleinermanns, K.; González, L.; Beckert, R. *Dyes Pigm.* **2012**, *94*, 512−524.
(33) Menzel, R.; Kupfer, S.; Mede, R.; Weiß, D.; Görls, H.; González, L.; Beckert, R. *Euro. J. Organ. Chem.* **2012**, *27*, 5231−5247.

(34) Wächtler, M.; Guthmuller, J.; González, L.; Dietzek, B. *Coord. Chem. Rev.* **2012**, *256*, 1479−1508.

(35) Guthmuller, J.; Champagne, B. *J. Chem. Phys.* **2007**, *127*, 164507-1−164507-11.

(36) Mennucci, B.; Cappelli, C.; Guido, C. A.; Cammi, R.; Tomasi, J. *J. Phys. Chem. A* **2009**, *113*, 3009−3020.

(37) Boereboom, J. M.; van Hemert, M. C.; Neugebauer, J. *Chem. Phys. Chem.* **2011**, *12*, 3157−3169.

(38) Silverstein, D. W.; Jensen, L. *J. Chem. Theory Comput.* **2010**, *6*, 2845−2855.

(39) Santoro, F.; Cappelli, C.; Barone, V. *J. Chem. Theory Comput.* **2011**, *7*, 1824−1839.

(40) Ma, H.; Liu, J.; Liang, W. *J. Chem. Theory Comput.* **2012**, *8*, 4474−4482.

(41) Guthmuller, J.; González, L. *Phys. Chem. Chem. Phys.* **2010**, *12*, 14812−14821.

(42) Tschierlei, S.; Karnahl, M.; Presselt, M.; Dietzek, B.; Guthmuller, J.; González, L.; Schmitt, M.; Rau, S.; Popp, J. *Angew. Chem., Int. Ed.* **2010**, *49*, 3981−3984.

(43) Kupfer, S.; Guthmuller, J.; Wächter, M.; Losse, S.; Rau, S.; Dietzek, B.; Popp, J.; González, L. *Phys. Chem. Chem. Phys.* **2011**, *13*, 15580−15588.

(44) Menzel, R.; Täucher, E.; Weiß, D.; Beckert, R.; Görls, H. *Z. Anorg. Allg. Chem.* **2010**, *636*, 1380−1385.

(45) Otsubo, T.; Aso, Y.; Takimiya, K. *J. Mater. Chem.* **2002**, *12*, 2565−2575.

(46) Kim, E.; Park, S. B. *Chem.—Asian J.* **2009**, *4*, 1646−1658.

(47) Jose, J.; Burgess, K. *Tetrahedron* **2006**, *62*, 11021−11037.

(48) Duan, L.; Qiao, J.; Sun, Y. D.; Qiu, Y. *Adv. Mater.* **2011**, *23*, 1137−1144.

(49) Menzel, R.; Breul, A.; Pietsch, C.; Schäfer, J.; Friebe, C.; Täuscher, E.; Weiß, D.; Dietzek, B.; Popp, J.; Beckert, R.; Schubert, U. S. *Macromol. Chem. Phys.* **2011**, *212*, 840−848.

(50) Reinhardt, B. A.; Brott, L. L.; Clarson, S. J.; Dillard, A. G.; Bhatt, J. C.; Kannan, R.; Yuan, L.; He, G. S.; Prasad, P. N. *Chem. Mater.* **1998**, *10*, 1863−1874.

(51) Oliva, M. M.; Casado, J.; Raposo, M. M.; Fonseca, A. M.; Hartmann, H.; Hernández, V.; Navarrete, J. T. L. *J. Org. Chem.* **2006**, *71*, 7509−7520.

(52) Happ, B.; Schäfer, J.; Menzel, R.; Hager, M. D.; Winter, A.; Popp, J.; Beckert, R.; Dietzek, B.; Schubert, U. S. *Macromolecules (Washington, DC, U. S.)* **2011**, *44*, 6277−6287.

(53) Becke, A. D. *J. Chem. Phys.* **1993**, *98*, 5648−5652.

(54) Lee, C.; Yang, W.; Parr, R. G. *Phys. Rev. B* **1988**, *37*, 785−789.

(55) Hariharan, P. C.; Pople, J. A. *Theor. Chim. Acta* **1973**, *28*, 213−222.

(56) Pierloot, K.; Dumez, B.; Widmark, P.-O.; Roos, B. O. *Theor. Chim. Acta* **1995**, *90*, 87−114.

(57) Aquilante, F.; Malmqvist, P.-Å.; Pedersen, T. B.; Ghosh, A.; Roos, B. O. *J. Chem. Theory Comput.* **2008**, *4*, 694−702.

(58) Malmqvist, P.-Å.; Roos, B. O. *Chem. Phys. Lett.* **1989**, *155*, 189−194.

(59) Frisch, M. J.; Trucks, G. W.; Schlegel, H. B.; Scuseria, G. E.; Robb, M. A.; Cheeseman, J. R.; Scalmani, G.; Barone, V.; Mennucci, B.; Petersson, G. A.; Nakatsuji, H.; Caricato, M.; Li, X.; Hratchian, H. P.; Izmaylov, A. F.; Bloino, J.; Zheng, G.; Sonnenberg, J. L.; Hada, M.; Ehara, M. T., K.; Fukuda, R.; Hasegawa, J.; Ishida, M.; Nakajima, T.; Honda, Y.; Kitao, O.; Nakai, H.; Vreven, T.; Montgomery, J. A., Jr.; Peralta, J. E.; Ogliaro, F.; Bearpark, M.; Heyd, J. J.; Brothers, E.; Kudin, K. N.; Staroverov, V. N.; Kobayashi, R.; Normand, J.; Raghavachari, K.; Rendell, A.; Burant, J. C.; Iyengar, S. S.; Tomasi, J.; Cossi, M.; Rega, N.; Millam, N. J.; Klene, M.; Knox, J. E.; Cross, J. B.; Bakken, V.; Adamo, C.; Jaramillo, J.; Gomperts, R.; Stratmann, R. E.; Yazyev, O.; Austin, A. J.; Cammi, R.; Pomelli, C.; Ochterski, J. W.; Martin, R. L.; Morokuma, K.; Zakrzewski, V. G.; Voth, G. A.; Salvador, P.; Dannenberg, J. J.; Dapprich, S.; Daniels, A. D.; Farkas, Ö.; Foresman, J. B.; Ortiz, J. V.; Cioslowski, J.; Fox, D. J. *Gaussian 09*, revision A.02; Gaussian, Inc.: Wallingford, CT, 2009.

(60) Aquilante, F.; Vico, L. D.; Ferré, N.; Ghigo, G.; Malmqvist, P.-Å.; Neogrády, P.; Pedersen, T. B.; Pitonak, M.; Reiher, M.; Roos, B. O.; Serrano-Andrés, L.; Urban, M.; Veryazov, V.; Lindh, R. *J. Comput. Chem.* **2010**, *31*, 224−247.

(61) Veryazov, V.; Widmark, P. O.; Serrano-Andrés, L.; Lindh, R.; Roos, B. O. *Int. J. Quantum Chem.* **2004**, *100*, 626−635.

(62) Karlström, G.; Lindh, R.; Malmqvist, P.-Å.; Roos, B. O.; Ryde, U.; Veryazov, V.; Widmark, P. O.; Cossi, M.; Schimmelpfennig, B.; Neogrády, P.; Seijo, L. *Comput. Mater. Sci.* **2003**, *28*, 222−239.

(63) Heller, E. J.; Sundberg, R.; Tannor, D. *J. Phys. Chem.* **1982**, *86*, 1822−1833.

(64) Merrick, J. P.; Moran, D.; Radom, L. *J. Phys. Chem.* **2007**, *111*, 11683−11700.

(65) Johnson, R. D., III. Comparison, N. C. C.; Database, B.; NIST Standard Reference Database Number 101, Release 15b, August 2011.

(66) Tozer, D. J. *J. Chem. Phys.* **2003**, *119*, 12697−12699.

(67) Autschbach, J. *Chem. Phys. Chem.* **2009**, *10*, 1757−1760.

(68) Kuritz, N.; Stein, T.; Baer, R.; Kronik, L. *J. Chem. Theory Comput.* **2011**, *7*, 2408−2415.

(69) Guillaume, M.; Champagne, B.; Zutterman, F. *J. Phys. Chem. A* **2006**, *110*, 13007−13013.

(70) Guthmuller, J.; Zutterman, F.; Champagne, B. *J. Chem. Theory Comput.* **2008**, *4*, 2094−2100.

(71) Marder, S. R.; Perry, J. W.; Bourhill, G.; Gorman, C. B.; Tiemann, B. G.; Mansour, K. *Science* **1993**, *261*, 186−189.